Earth Surf. Dynam., 9, 1335–1346, 2021
https://doi.org/10.5194/esurf-9-1335-2021

Earth Surface Dynamics
Open Access
EGU

Sediment shell-content diminishes current-driven sand ripple development and migration

Chiu H. Cheng[1,2], Jaco C. de Smit[1,3], Greg S. Fivash[1], Suzanne J. M. H. Hulscher[4], Bas W. Borsje[4], and Karline Soetaert[1]

[1]Department of Estuarine and Delta Systems (EDS), NIOZ Royal Netherlands Institute for Sea Research, 4400 AC Yerseke, the Netherlands
[2]Wageningen Marine Research, Wageningen University & Research, 4400 AB Yerseke, the Netherlands
[3]Department of Physical Geography, Faculty of Geosciences, Utrecht University, 3584 CB Utrecht, the Netherlands
[4]Water Engineering and Management, University of Twente, 7500 AE Enschede, the Netherlands

Correspondence: Chiu H. Cheng (chiu.cheng@nioz.nl)

Received: 18 February 2021 – Discussion started: 2 March 2021
Revised: 29 July 2021 – Accepted: 10 September 2021 – Published: 7 October 2021

Abstract. Shells and shell fragments are biogenic structures that are widespread throughout natural sandy shelf seas and whose presence can affect the bed roughness and erodibility of the seabed. An important and direct consequence is the effect on the formation and movement of small bedforms such as sand ripples. We experimentally measured ripple formation and the migration of a mixture of natural sand with increasing volumes of shell material in a racetrack flume. Our experiments reveal the impacts of shells on ripple development in sandy sediment, providing information that was previously lacking. Shells expedite the onset of sediment transport while simultaneously reducing ripple dimensions and slowing down their migration rates. Moreover, increasing shell content enhances near-bed flow velocity due to the reduction of bed friction that is partly caused by a decrease in average ripple size and occurrence. This, in essence, limits the rate and magnitude of bed load transport. Given the large influence of shell content on sediment dynamics as well as the high shell concentrations found naturally in the sediments of shallow seas, a significant control from shells on the morphodynamics of sandy marine habitats is expected.

1 Introduction

Ripples are the most common bedforms found in the marine environment, including in shallow, sandy environments (Bartholdy et al., 2015; Langlois and Valance, 2007). They form over a broad range of sandy grain mixtures under low-energy flow or wave conditions that exceed the erosion threshold (Precht and Huettel, 2003; Soulsby, 1997). With increasing water depth, ripples become progressively driven by currents rather than waves. Current-generated ripples are very dynamic microscale bedforms, with typical sizes of around 0.1 m in wavelength and up to 0.01 m or more in height (Ashley et al., 1990; van Rijn et al., 1993). They continuously develop and erode, typically on the order of minutes to days, and can migrate at rates exceeding 0.4 cm min^{-1} (Baas et al., 2000; Baas and De Koning, 1995; Bartholdy et al., 2015; Lichtman et al., 2018). As the ripples move and change in dimension, the bed roughness is correspondingly altered, which can have cascading effects on the surrounding areas such as larger bedforms (e.g., tidal sand waves) on which they are often superimposed (Brakenhoff et al., 2020; Damveld et al., 2018, 2019; Idier et al., 2004). Additionally, ripples also generate distinct spatial variations in sediment composition and alter the distribution of particulate organic matter by their effect on hydrodynamics, some of which can further modify the sediment properties in ways that influence erosion (Ahmerkamp et al., 2015; Kösters and Winter, 2014; Mietta et al., 2009).

Shells, a biogenic material created by marine bivalves, are widely distributed in certain regions of the marine environment (Russell-Hunter, 1983). These calcareous structures remain present long after the death of the organisms (Gutiérrez et al., 2003; Kidwell, 1985), and they are mostly found in the form of separated individual shell valves and shell fragments. In environments where shells are prevalent, they may constitute 20 %–70 % of the total sediment composition (by volumetric percentage), although even higher percentages have been observed in very extreme cases (Dey, 2003; Soulsby, 1997). As they have a lower bulk density, their presence reduces the bulk density of the sediment by diluting the quartz fraction (Soulsby, 1997). As shell material is rather plate-like, irregular and angular in shape, they also change the general composition compared with the smaller, surrounding sediment particles (Al-Dabbas and McManus, 1987). Intact shells and larger fragments may inhibit sediment transport through bed armoring. Armoring occurs when the mean shear stress is below the critical erosion threshold for the coarsest fractions but above that for the finer particles, resulting in their entrainment. This winnowing causes the surface to become coarser and coarser, essentially building up an armor layer (Vericat et al., 2006). In riverine environments, coarse material such as gravel has been shown to facilitate bed armoring, causing the upper layers of the sediment to become significantly coarser than the median grain size (D_{50}) of the sediment beneath, ultimately reducing or inhibiting sediment transport (Curran, 2010; Wilcock and Detemple, 2005). Shells may also be able to provide a similar armoring effect against sand erosion given that they are more difficult to erode (Miedema and Ramsdell, 2011; Ramsdell and Miedema, 2010).

Thus far, very few studies have investigated the direct influence of shell material on the bed load transport dynamics through the alteration of bed roughness (Gutiérrez et al., 2003; Nowell and Jumars, 1984). Some studies have explored the ways in which shells could be used as tracers for sediment motion, given their widespread occurrence (Al-Dabbas and McManus, 1987). The drag and incipient motion of the valves of a few bivalve species have also been investigated in the laboratory (Dey, 2003). Similar studies have focused on the erosion and settling velocities of shells, based on shapes, shell positioning and associated drag, being transported through a pipeline (Miedema and Ramsdell, 2011; Ramsdell and Miedema, 2010). Although these studies have considered how the irregularity in shape and orientation of shell valves potentially interact with flow, the focus has been more within a hydrodynamic context rather than a sedimentary one. To our knowledge, no existing studies have addressed the direct effects of a natural, representative mixture of shells and sandy sediment on the development and movement of ripples.

From a hydraulic point of view, biogenic materials such as shells do not exhibit the same response as rock fragments of a similar size, although some shells (e.g., the mussel family, Mytilidae) have been shown to behave more similarly to the smaller sand particles (Al-Dabbas and McManus, 1987). However, due to the shape and size of most shells, combined with their lower density, they are known to have a much lower settling velocity and much larger erosion velocity threshold than sand particles (Ramsdell and Miedema, 2010). The mere presence of empty shells has also been shown to facilitate silt and other fine-particle entrainment in the sediment (Huettel and Rusch, 2000; Pilditch et al., 1997; Witbaard et al., 2016). Nevertheless, despite their prevalent nature and potential to affect sediment dynamics in several ways, there is currently a knowledge gap in terms of the direct influence of shells on the geomorphology of sandy sediments.

The objective of this experiment was to determine the effect of biogenic shells on the development of ripples in medium sand, in relation to unidirectional flow and turbulence along the bed. The combination of flow velocity and turbulence intensity largely dictates the sediment dynamics, thereby affecting bedform development and sediment stability (Blanchard et al., 1997; Herman et al., 2001; Paterson et al., 2001). Bottom roughness and small-scale topography are important contributing factors to bedform pattern development (Van Oyen et al., 2010), and past studies have found a significant effect of epibenthic structures at different densities (e.g., mimics of tube worm reef patches) on flow and sediment erosion (Friedrichs et al., 2000, 2009). However, the influence of shell material on the ripple dynamics, in relation to flow and turbulence, is still not well understood. Thus, we aimed to quantify the turbulence generated by the flow along sand ripples, simulating scenarios both with and without the presence of shells. We used shells from common bivalve species found in the sandy Dutch North Sea, including *Spisula* spp., *Tellimya* spp. and *Cerastoderma edule*, at increasing densities. Using empty shells, we determined the influence, via autogenic engineering, of shell material on sediment transport by testing the effects of increasing shell content on ripple formation, shape and migration rates.

Our paper is organized as follows: the experimental setup, instrumentation and analyses utilized are described in Sect. 2; the results, including the incipient sediment motion, ripple migration and other ripple calculations are presented in Sect. 3; the significance of our findings are discussed in Sect. 4; and Sect. 5 presents the final conclusions.

2 Materials and methods

2.1 The experimental setup

Our experiments were performed in a racetrack flume facility located at the NIOZ Royal Netherlands Institute for Sea Research, Yerseke, the Netherlands. This large, unidirectional flow channel measures approximately 17.5 m in length and 3.25 m in width and can generate depth-averaged currents of up to 60 cm s^{-1} (Fig. 1a). A test section containing a sedi-

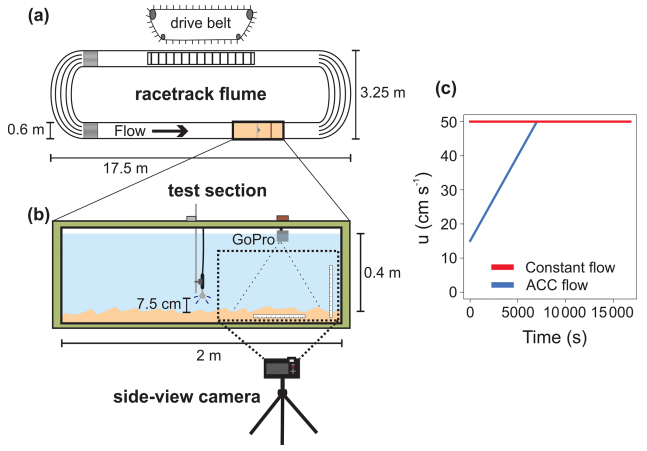

Figure 1. **(a)** The top view of the NIOZ racetrack flume. **(b)** A side view of the 2 m long test section showing the Nortek Vectrino® acoustic Doppler velocimeter (ADV), GoPro and side-view cameras used in each experimental run. Both cameras were positioned within the second half of the viewing window of the test section. **(c)** The flume flow settings implemented in the two separate experiments. Note that although ripples are shown for illustrative purposes, the indicated water depth and ADV height are based on the initial (flat bed) condition.

ment basin measuring 200 cm × 60 cm × 25 cm ($L \times W \times H$) is located at the far end of one of the long, straight sections of the flume to minimize the effect of bend flows (Fig. 1b). The drive belt equipped on the backside allows the flow to be controlled with high precision.

The basin of the 2 m test section was filled using North Sea sandy sediment (see Table S1 in the Supplement for the properties). To maintain a sediment supply throughout the duration of each individual experiment, a thin layer of sand (∼ 3 cm) was also placed over the 3 m preceding the measurement section of the flume track. The bed was fully mixed and flattened before each experimental run. The total water depth was 40 cm and only freshwater was used.

For the shell treatments, we used a mixture that consisted of, on average, approximately 29 % intact shells valves and 71 % fragments (in absolute number of pieces). All non-shell materials (e.g., rocks and wood detritus) were removed prior to the addition. We took a random sampling of the shell stockpile to determine the average dimensional properties of the shell valves and fragments (Table S2 and Fig. S1 in the Supplement).

Two separate experiments were conducted: a constant flow experiment was used to measure equilibrium ripple dimensions and migration rates, and an acceleration (ACC) flow experiment was run to measure the incipient sediment motion. The flow settings used in the two experiments are shown in Fig. 1c. Both experiments consisted of several experimental runs, which were varied by changing the volumetric percentage of shell content. The control (0 % shells) contained only sandy sediment, while each subsequent treatment was modified by the addition of shell material. The volumetric percentage of shell increased by 2.5 % or 5 % intervals, up to 30 %, while the last two treatments contained 40 % and 50 % shell, respectively. The flume was filled with water overnight, and all experimental runs were always performed the very next day to maintain consistency (e.g., minimize variability due to factors such as compaction). The constant flow experiment consisted of six treatments (0 %, 5 %, 10 %, 15 %, 20 % and 50 % shell), whereas the ACC flow experiment included 11 treatments (0 %, 2.5 %, 7.5 %, 10 %, 12.5 %, 15 %, 20 %, 25 %, 30 %, 40 % and 50 %; see Table S3 for a summary of the experimental settings and measurements).

2.2 Constant flow experiment

In the constant flow experimental runs, a 50 cm s^{-1} depth-averaged flow velocity was maintained for more than 4 h so as to achieve equilibrium conditions (Fig. 1c). Preliminary runs showed that morphological equilibrium was achieved well within 1 h at this flow rate. A Canon EOS 1000D camera, equipped with an EX Sigma lens (DG Macro, 50 mm, 1 : 2.8) was positioned at the side of the flume, targeting the second half of the test section to record time-lapse photos from the side at 10 s intervals. The photos recorded a section that was 76.5 cm in width and 51 cm in height. Two rulers were attached at the edges of the frame as dimensional guides for the image analyses (Fig. 1b).

Concurrently, a Nortek Vectrino® acoustic Doppler velocimeter (ADV) profiler was used to record the three-dimensional flow rates, through coherent Doppler processing, at a frequency of 30 Hz. Data were filtered for minimum correlation values of 90 %, minimum signal-to-noise ratio of 20 dB and minimum amplitude of −35 dB. The probe was placed approximately 7.5 cm above the bed, which was initially flat in each experimental run. With a blanking distance of 4 cm, it measured the bottom section of the water column from 0 to 3.5 cm above the initial flat bed, over a total of 35 cells (1 mm intervals). The ADV was held in place through the duration of the experimental run. Therefore, near-bed flow profiles were corrected for changing bed elevation during ripple migration.

2.3 Sediment image processing

Identification of ripples within the sediment bed was performed through image analysis of the photo time-series obtained by the camera. The vertical position of the sediment-water interface was identified using Canny edge detection of the green band with the "wvtool" R package (Sugiyama and Kobayashi, 2016), which showed the highest contrast. Gamma transformation of the green band further enhanced this contrast to improve the quality of the detection. The fine-grain noise in the sediment surface was filtered out using a low-pass second-order Butterworth filter to produce a smooth surface from which peaks and troughs can be easily identi-

fied, using the "signal" R package (Ligges et al., 2015). Ripples were then classified from the identified sediment surface using peak analysis, which isolated peaks and troughs in the sediment surface with the "pracma" R package (Borchers, 2019). This ultimately allowed us to characterize the dimensions of individual ripples and track their movement and development in time. Using 1600 unique frames from each of the six constant flow experimental runs, we quantified the following ripple parameters: (1) the ripple height, (2) length, (3) asymmetry and (4) migration rate.

Each ripple was defined as encompassing the region between two neighboring troughs, separated by a peak. The ripple height and length were defined as the maximum vertical and lateral extent of the ripple. The ripple asymmetry was defined as the difference in length between the two halves of the ripple, separated by the center of its peak, divided by its total length (trough–trough): values change from 0 (highest symmetry) to 1 (highest asymmetry). The migration rate was calculated as the total distance traveled by the peak of a unique ripple over 24 frames (constituting an interval of 4 min). This frame interval allowed ripples to travel measurable distances while limiting the likelihood of them moving out of frame before measurements could be taken. All four of the ripple parameters were measured throughout the experimental duration using each frame. Only whole ripples were used in the analyses: ripples that were partially in (upstream) or out (downstream) of the frame were excluded. Given that the migration rate was calculated over 24 frames, measurements were not generated from the first or last 23 frames in each run. All image analyses were conducted in R version 3.4.4 (R Core Development Team, 2020).

2.4 Near-bed flow calculations

The near-bed turbulent kinetic energy (TKE) was derived from the near-bed flow velocity fluctuations (Pope et al., 2006). This value indicates the mean kinetic energy associated with eddies from the turbulent flow. It is a more robust method for determining the bed shear stress than techniques such as quadrant analysis or Reynold's stress, as these are highly sensitive to the orientation of the ADV profiler. The near-bed TKE was calculated from near-bed flow velocity fluctuations in the x, y and z directions as follows:

$$\mathrm{TKE} = \frac{1}{2}\left(\overline{u'^2_{b,x}} + \overline{u'^2_{b,y}} + \overline{u'^2_{b,z}}\right), \quad (1)$$

where $\overline{u'_{b,x}}$, $\overline{u'_{b,y}}$ and $\overline{u'_{b,z}}$ represent the root mean squares of the near-bed flow velocity fluctuations in the x, y and z directions, respectively. These values were extracted from the flow velocity signal through means of applying a 0.1 Hz high-pass fifth-order Butterworth filter. This ensures removal of the background velocity during the measurement period. Another 10 Hz low-pass fifth-order Butterworth filter was used to remove the higher frequencies where the signal was dominated by noise. The corresponding bottom shear stress (BSS) was calculated as follows (Soulsby, 1983):

$$\mathrm{BSS} = 0.19\rho\mathrm{TKE}, \quad (2)$$

where ρ is the water density (1000 kg m^{-3} for freshwater). Subsequently, the corresponding total bed roughness, which is affected by both shells and bed forms, can be calculated from the depth-averaged velocity and the BSS. For a unidirectional flow, the BSS can be calculated from the depth-averaged velocity as follows (van Rijn, 1993):

$$\mathrm{BSS} = \rho g \frac{u^2}{C^2}, \quad (3)$$

where u is the depth-averaged velocity (m s^{-1}), g is the gravitational acceleration (9.81 m s^{-2}) and C is the Chézy roughness coefficient (m$^{0.5}$ s^{-1}). The Chézy roughness coefficient is a function of the water depth and bed roughness (van Rijn, 1993):

$$C = 18\log\left(\frac{12h}{ks}\right), \quad (4)$$

where h is the water depth (0.4 m in this flume experiment), and ks is the total bed roughness (m) by combined grain friction and form drag.

2.5 ACC flow experiment

This experiment was conducted to measure the onset of incipient sediment transport, as well as the corresponding boundary layer conditions. Incipient sediment transport was measured for a flat bed configuration in order to quantify the direct effect of shells on sediment stability. Sandy sediment with a D_{50} of 350 µm is not expected to exhibit sediment motion below about 30 cm s^{-1} (van Rijn, 1993), and an initial test run with our setup showed that there was indeed no sediment movement occurring below 20 cm s^{-1}. Thus, the starting velocity of each run was set at 15 cm s^{-1}. The flow speed was linearly increased at a rate of 0.3 cm s^{-1} min^{-1} from 15 to 50 cm s^{-1} (over a time frame of 116.6 min).

The ADV profiler was again anchored in the middle of the test section. One GoPro HERO3 camera was positioned just below the water surface, looking downward, 1.5 m along the test section to produce top-view video recordings of the sediment surface at 2 frames per second. The onset of incipient motion, which was defined as the frequent movement of particles across the entire flume area, was derived visually from the GoPro footage (van Rijn, 1993). Visual observation is an accurate method to determine erosion thresholds. As bed load transport is proportional to flow velocity to the power of 3, a small change in velocity will lead to a significant and easily observable change in sediment transport. The depth-averaged velocity was determined from the flume setting at the identified time when incipient motion was observed (Fig. 1c). The critical mean near-bed flow velocity,

TKE and BSS were derived from the ADV measurements over the 5 min preceding and the 5 min after the onset of incipient motion following Eqs. (1) and (2). The total bed roughness for flat beds with varying shell content was calculated following Eqs. (3) and (4), using a 10 min window of ADV measurements at an average flow rate of 20 cm s^{-1}, before any ripples had formed.

3 Results

We tested a large range of shell content in our constant flow experiment, and the results clearly demonstrate that the reduction of ripples is strongly correlated with the shell fraction of sandy sediments. Consequently, the ripple height, length and migration rate were all significantly reduced by the increasing shell content, while the ripple shape became slightly more asymmetric. In the constant flow experiments, the ripples appeared to achieve equilibrium conditions within the first hour at a flow rate of 50 cm s^{-1}. The change in ripple length and height, in particular, can clearly be seen in the concluding frames of each experimental run, particularly around 20 % shell content in the constant flow experiment (Fig. 2a). The ripple height, length, asymmetry and migration rate were not measured in the ACC flow experiment, as we were interested in determining the incipient motion from these runs. Nevertheless, a similar observation could still be seen at around 15 % shell content, even though these ripples were less equilibrated given the lower flow rates for much of the experimental duration (Fig. 2b). In addition, as the shell percentage increased in the experimental runs, they began to exhibit larger, denser aggregations (Fig. 3). What appeared to be bands of shells were actually immobile surficial shells that would periodically appear or disappear as ripples migrated over them. Furthermore, the already smaller ripples were observed (from the GoPro videos) to either migrate around the denser and slightly higher positioned shells or to disappear altogether, so the shells did not incorporate themselves into the (migrating) ripples. Even in the lower shell concentrations, where larger ripples frequently migrated over the sparser quantity of shells, the vast majority of these surficial shells were not moved by the moving ripples nor by the flow (Fig. S2). By performing two types of measurements, we investigated both the (theoretical) equilibrium situation at constant high-flow conditions (50 cm s^{-1}) and the sequence of events that occur as the velocity increases (the ACC flow experiment). The latter pointed to the physical conditions under which sediment dynamics begin to change (e.g., incipient motion).

3.1 Changes to ripple characteristics (constant flow experiment)

An increase in the shell percentage reduced the spatial dimensions of the ripples, and all of the ripple parameters, except ripple symmetry, were highly affected by the presence of shells. The ripple height, length and migration rate all decreased exponentially as a function of shell content, such that the ripples almost entirely disappeared at 50 % shell content (Fig. 2). The ripples also became slightly more asymmetric with increasing shell content (Fig. 4c). Overall, the lengths and heights of the ripples decreased at an average rate of −0.03 cm per percentage point of shell for the height, and −0.16 cm per percentage point of shell for the length (Fig. 4a, b). Ripple asymmetry increased at an average rate of 0.002 per percentage point of shell (Fig. 4c). The migration rate showed a consistent decrease with increasing shell content, slowing at an average rate of -0.016 cm min^{-1} per percentage point of shell (Fig. 4d). Approximately 18, 20, 14, 13, 13 and 12 ripples were included in the calculations for each experimental run (from 0 % to 50 % shell content; Fig. S3).

3.2 Changes to near-bed hydrodynamics and critical BSS

In the constant flow experiment, the presence of shells (at all percentages) enhanced the near-bed flow in the streamwise direction (Fig. 5a), as ripple sizes became diminished (Fig. 4). Near-bed vertical flow was, on average, directed downwards and decreased with increasing shell content (Fig. 5b). Interestingly, while the increasing near-bed flow velocity with increasing shell percentages indicates a reduction in overall bed friction (Fig. 5a), the highest TKE is observed at 50 % shell content (Fig. 5c). Overall, there is also a consistent pattern in the turbulent structure maintained between each run (Fig. S4).

The critical near-bed velocity profiles from the ACC flow experimental runs showed a large reduction in critical near-bed velocity between 0 % and 15 % shell content, followed by a minor reduction towards the 50 % shell content (Fig. 6a). No differences were observed between the vertical velocity profiles (Fig. 6b), which averaged zero as the ripples were absent. Shells had a strong influence on the critical TKE and BSS (Fig. 7a). The most immediate and drastic changes in the critical BSS occurred when the smallest quantity of shell was mixed into the sediment (2.5 %), where the addition of shell material initially increased the critical BSS from approximately 0.2 N m^{-2} at 0 % shell content to approximately 0.75 N m^{-2} at 2.5 % shell content (Fig. 7a). Subsequently, the critical BSS dropped towards 0.25 N m^{-2} at 15 % shell content ($R^2 = 0.91$; Fig. 7a). At shell concentrations above 20 %, the critical BSS slowly increased again to approximately 0.5 N m^{-2} at 50 % shell content ($R^2 = 0.50$; Fig. 7a). In contrast to the critical BSS, the critical depth-averaged velocity for incipient motion consistently reduced towards 15 % shell content ($R^2 = 0.99$; Fig. 7b), after which it remained constant ($R^2 = 0.29$; Fig. 7b). The quadrant analysis plots show that the turbulence-induced flow is predominantly directed forwards and downwards (Fig. S5).

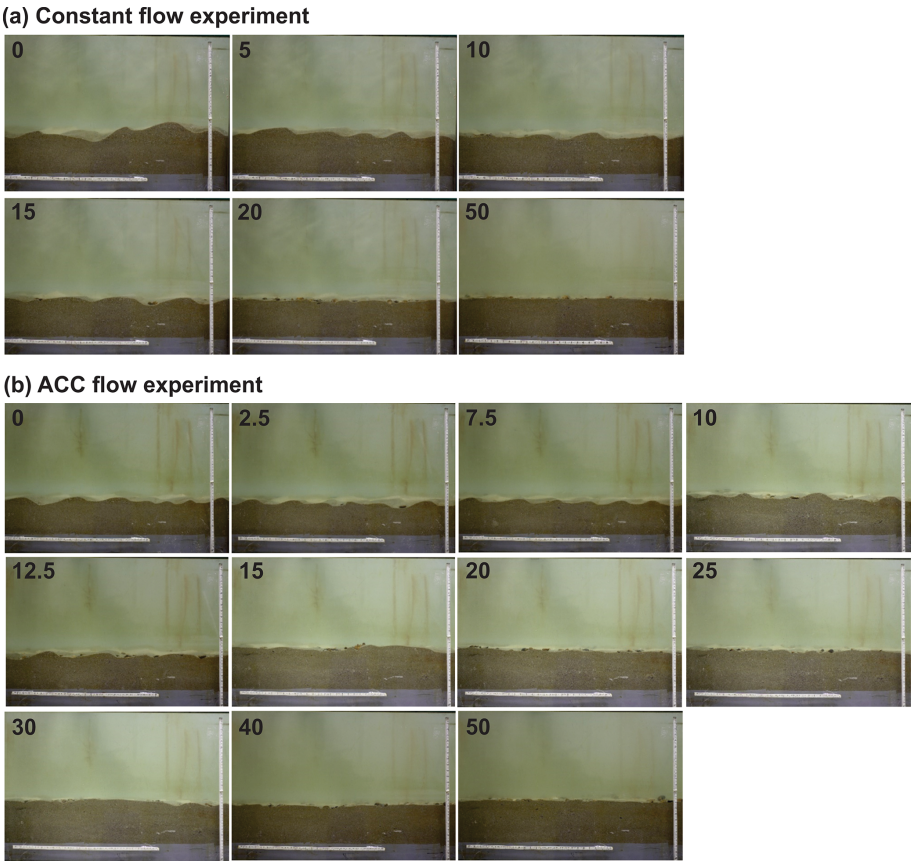

Figure 2. The final frame from each **(a)** constant flow and **(b)** ACC flow experimental run. Numbers represent the shell percentage. The white vertical and horizontal rulers are both 50 cm in length.

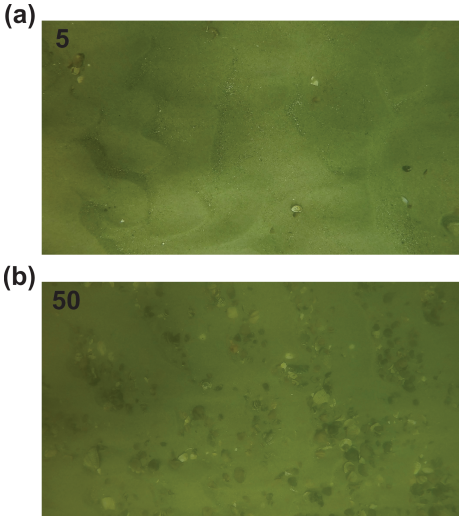

Figure 3. Stills taken from the GoPro videos (constant flow experiment) to show the contrast between a **(a)** low-density and **(b)** high-density treatment. Shells increasingly appear as immobile clusters at higher concentrations, as they are periodically exposed due to sand movement. The numbers represent the shell percentage.

The influence of shells on the total bed roughness showed contrasting behavior between flat (e.g., ACC flow experiment) and equilibrium (e.g., constant flow experiment) beds (Fig. 8). In the absence of bed forms, the total bed roughness showed a similar trend to the critical BSS: a large increase from 1.2×10^{-4} to 0.042 m between 0 % and 7.5 % shell content, followed by a decrease to 0.007 m at 15 % shell content, after which it stabilized at 0.005 ± 0.004 m towards 50 % shell content. When ripples were present (equilibrium bed), the total bed roughness decreased from 0.02 to 0.013 m at 0 % to 10 % shell content. Beyond 10 % shell content, the total bed roughness increased to 0.036 m.

4 Discussion

4.1 Significance of shell–ripple interactions

In gravel bed rivers, it is known that the incorporation of topography into the sediment surface creates microclusters that increase both the bed roughness and bed stability (Curran, 2010). The anchoring of shells, even through partial burial, in sandy sediment greatly raises their critical erosion threshold compared with individual shells situated on a flat surface,

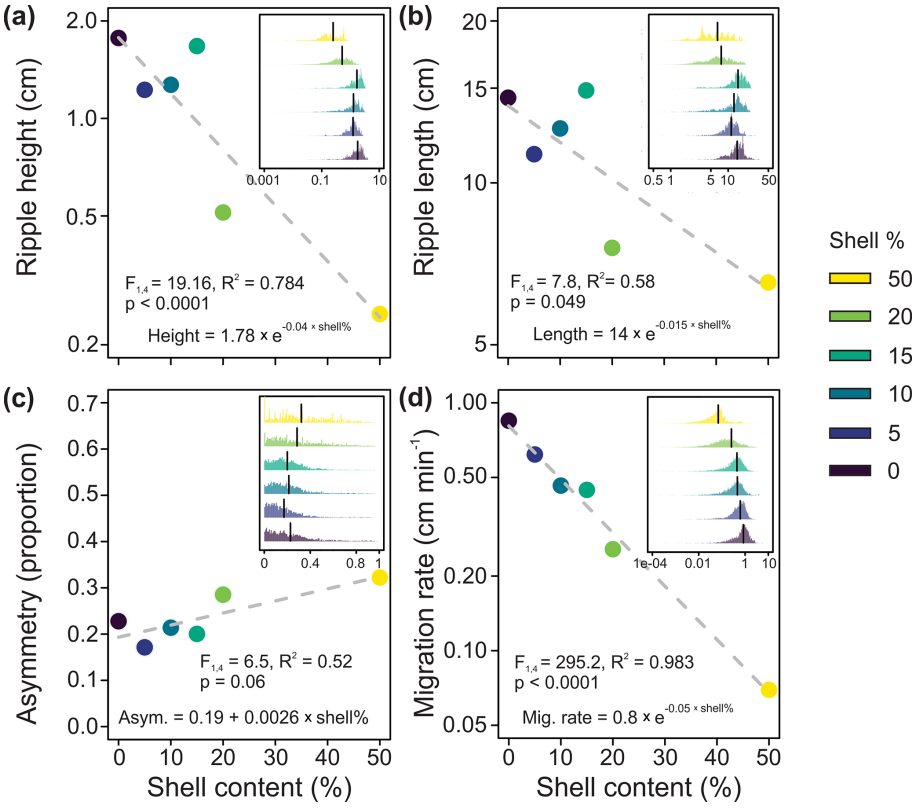

Figure 4. **(a)** Ripple height, **(b)** ripple length, **(c)** asymmetry and **(d)** migration rate, plotted against the shell content from the constant flow experimental runs ($n = 6$). The y axis of the ripple height, length and migration are plotted on a log scale. The inset panels show the corresponding histograms for each ripple parameter, with the x axis values representing the y axis values of the respective regression plots. Vertical lines represent mean values.

irrespective of the orientation. Whereas loose shells on top of a flat sandy surface can erode at velocities well below 40–50 cm s^{-1} (Dey, 2003), shells that are fixed in the sediment, especially in clusters, are much less susceptible to erosion. In our experiments, the shells were almost completely immobile over the entire duration of the experimental runs, with no visually noticeable change as evidenced by both the time series photos and video footage (Fig. S2). What would appear as bands of shell is an artifact caused by the localized changes and movement of the sand, rather than a change to the shells. Despite flow velocities reaching these thresholds in our experiments, the shells were mostly immobile, even as ripples migrated over them. In rare cases, the smaller valves and fragments sometimes shifted a few centimeters due to ripple movement. However, in the higher shell concentration treatments, the shells were practically fixed structures (Figs. 3, S2).

Therefore, a sandy sediment bed with a sufficient quantity of shells under a unidirectional flow will produce an armoring effect somewhat similar to riverine environments, where gravel beds produce clustered structures that mediate the bed–flow interactions through a combination of bed stabilization, altered roughness and regulation of the amount of sediment available for transport (Curran, 2010; Tuijnder et al., 2009; Wilcock and Detemple, 2005). In addition, our experiments show that shell content has another indirect bed-mediating effect. Due to the dampening of the size of the ripples and the consequent reduction in bottom roughness, there was a progressive enhancement of the mean near-bed flow (Fig. 6) as a function of increased shell content and the concurrent slowdown of the ripple migration rate (Fig. 4d), due to both a decrease in overall sediment supply (from shell displacement) and immobile shells, even at the very low percentages.

The opposing behavior in terms of critical BSS and depth-averaged velocity indicates that shells may modify sediment-flow interactions in two ways: (1) by stabilizing the sediment, and (2) by increasing the total bed roughness and near-bed TKE. Following this, the large increase in critical BSS for low shell concentrations is probably a consequence of a large increase in sediment stability or a large increase in bed roughness, given that the reduction in critical depth-averaged velocity remains minimal. In the case of low shell density, shells may disrupt flow in the boundary layer, thereby increasing the TKE. For higher shell densities, flow may be deflected over the shells, which progressively reduces the

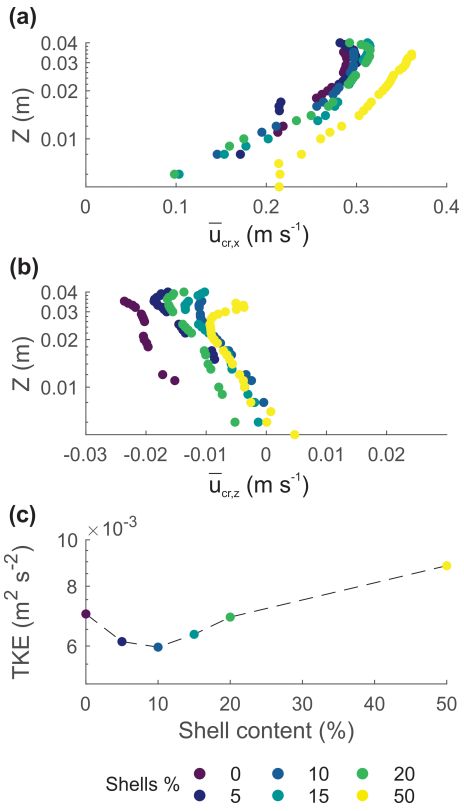

Figure 5. Time-averaged near-bed velocity profiles showing the **(a)** x and **(b)** z direction of the constant flow experimental runs as well as the **(c)** peak TKE values plotted against shell content. Note that the profiles are time-averaged, as indicated by the overbars, over the entire duration of each experimental run.

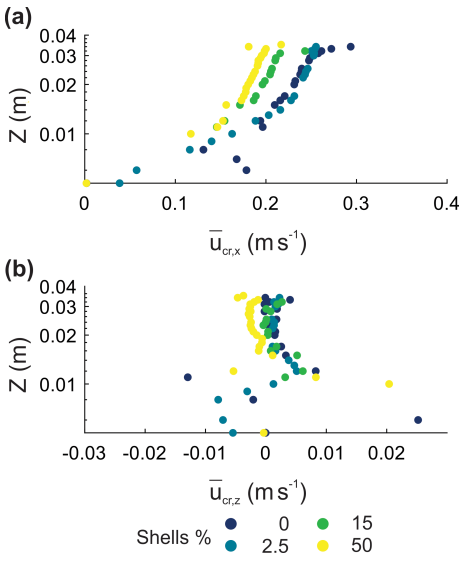

Figure 6. **(a)** Near-bed streamwise flow and **(b)** vertical flow at the onset of sediment transport for flat beds (ACC flow experiment). Note that the overbars denote that the x axes are time-averaged, over a 10 min period, which encompasses the 5 min prior to and following the incipient motion, for the four selected experimental runs.

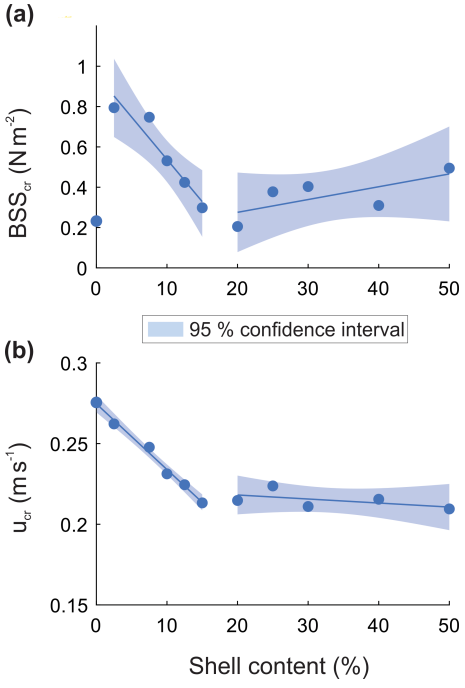

Figure 7. **(a)** The critical BSS for incipient motion and the **(b)** corresponding depth-averaged velocity for the ACC flow experiment. The shaded regions represent the 95th percentile confidence intervals.

disturbance of the boundary layer and, thus, the TKE. Similar density-dependent alterations in flow patterns from flume studies using either live animals or mimics have also been observed (Friedrichs et al., 2000, 2009). In these studies, the erosion fluxes and the deposition of suspended material were substantially enhanced when densities were such that less than 4 % of the sediment area was covered, whereas both factors saw a drastic reduction above this level of coverage.

As the flat bed transitions towards a rippled one, the initial flow and (de)stabilization effects begin to shift. As the shell content increases, the sand available for migration decreases while the immobile shells hamper ripple formation. Consequently, the attainable ripple size is negatively correlated with shell content. Both the presence of ripples and shells increase the bottom roughness, and the pattern of the calculated total bed roughness, which is minimal at intermediate shell content, shows both impacts. Bed roughness was actually the largest where the shell content was also highest (Fig. 8), despite the ripple size having diminished substantially. This contrasting pattern shows that, in the absence of ripples, small shell concentrations generate a high total bed roughness, but this effect is suppressed by the large rip-

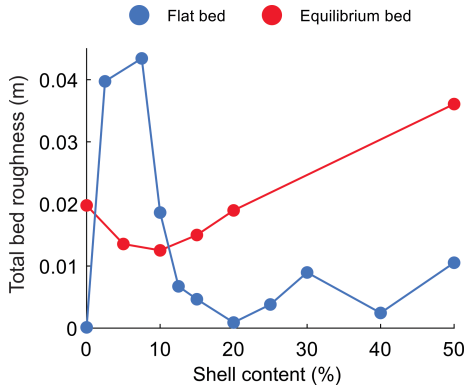

Figure 8. Total bed roughness against shell content for the flat beds (ACC flow experimental runs) and equilibrium beds (constant flow experimental runs).

ples that are formed under these conditions at equilibrium. At high shell concentrations, however, the direct effect of shells on total bed roughness is smaller, but when reinforced by the presence of small ripples, this results in a higher combined net roughness (Fig. 8).

4.2 Potential implications of shells for larger-scale sediment dynamics

Natural sediments rarely consist of pure, clean sand, and often include other debris, fragments and particles (Earle, 2020; Gornitz, 2008; Seibold and Berger, 2017). Nevertheless, sediment characteristics are important for bedform development, roughness and larger-scale implications, and even minute changes can immediately impact smaller bedforms such as sand ripples. Similar dampening effects have been shown for other biogenic substances and fine particles (Friend et al., 2008; van Ledden et al., 2004; Malarkey et al., 2015). Biogenic shells, given their size, density and dimensional aspects, behave very differently from sand grains (Soulsby, 1997), and, as shown here, a composition of 2.5 % shell can already drastically enhance critical BSS and total bed roughness. As the rippled bed matures, which is likely the realistic scenario in many sandy seabeds, the effects of increasing shell content becomes more evident, through patterns of bed stabilization (e.g., armoring). Our quantities of shell material are well within the range observed in sandy coastal environments. At a sandy (sand wave) location within the Dutch North Sea (Cheng et al., 2020; Damveld et al., 2018), the shell content of the sediment samples was also determined. We measured shell percentages ranging from < 1.0 % to 41 % (mean = 8 %, mode = 7 %). Given the observed complexity in the near-bed flow conditions at these shell percentages, this signifies that many such sandy environments are likely to be subjected to similar sand–shell–ripple interactions.

The primary mechanisms driving current-generated ripple dynamics are rather well established, but good indicators are still lacking for ripple size, which is dependent on the grain size, viscosity, density and flow strength (Lapôtre et al., 2017). Most model predictions typically omit other particle types or represent the sediment by a single value (e.g., D_{50}). However, given the fact that these shell valves and fragments differ in size, shape and density from sand grains and are largely immobile in our experiments, they cannot be accurately approximated by equations developed for average sand grains. Nevertheless, the addition and subsequent coarsening due to shell valves and fragments dampened the ripples up to 7-fold with height, more than 2-fold in length and with an order of magnitude reduction in migration rate (bare sand vs. 50 % shells; Fig. 4a, b, d). The effect of shells on ripple symmetry is inconclusive. There was a very slight increase in asymmetry, but this may be due more to the noise from the variability than to an actual trend (Fig. 4c).

We have shown how shell percentages of around 10 %–15 % already reduced ripple size significantly, and above 20 %, ripples are almost entirely absent. We also observed largely immobile clusters or bands of shells, essentially stabilizing the sediment through an armoring effect. This is perhaps most comparable with the riverine gravel-bed armoring phenomenon, where due to the coarser sediment particles and flow conditions, coarser grains are partitioned to the top. Consequently, the surface becomes a relatively immobile layer inhibiting sediment transport, among other hydrodynamic interactions (Curran, 2010; Dietrich et al., 1989; Shen and Lu, 1983; Tuijnder et al., 2009). Storm events are often necessary to cause significant flushing of the lower layers or even break an armored layer (Vericat et al., 2006). It would be interesting to investigate how a large quantity of immobile shells would behave under such extreme conditions. Some evidence suggests that gravel-bed armoring can persist through floods, but the level of mobility and partial replacement or renewal of grains in the surface layer is inconclusive (Wilcock and Detemple, 2005).

Care must be taken in drawing comparisons, as these are dissimilar environments with entirely different causes for the armoring. As mentioned above, the shells were already immobile from the start to finish in our experimental runs, and the long-term formation/evolution processes of sand–shell beds remain inconclusive. Moreover, unlike the riverine gravel, which is closer to a spherical shape, shells are an entirely separate class of materials with biological origins. Under typical unidirectional flow conditions, a higher shell percentage can be expected to dampen ripple development, migration and, consequently, the bed load transport. How shells might affect the hydrodynamics and bed morphology under more-complex systems and flow conditions, particularly in shallower, wave-dominated environments, remains to be investigated (e.g., under sheet or oscillatory flow conditions; Nelson et al., 2013; Precht and Huettel, 2003; Soulsby, 1997).

Nevertheless, we foresee many relevant implications of shell research in geomorphologic investigations as well as coastal engineering applications. Shells clearly have the ability to regulate ripple growth and migration and, consequently, the bed load transport. A good estimation of the sediment–shell composition would allow us to assess the sediment dynamics for a given sandy environment and provide better insight into bed stability to produce more accurate calculations of bed load transport. Concurrently, given the close coupling between sediment transport and larger-scale adaptations in seabed morphology, this information could aid in developing or utilizing better methods with regards to offshore seabed patterns, shoreline preservation, alongshore sediment transport and coastal management. Our study has provided new insight into how shell material directly, and measurably, influences ripple evolution and migration in medium sand.

5 Conclusions

A series of sand–shell–ripple experiments were conducted to directly measure the impact of shell material on the development of current-driven ripples in sandy sediment ($D_{50} = 352\,\mu m$). Our results demonstrate that the shell content has a dynamic effect on the near-bed hydrodynamics that changes over several stages. This mainly occurs as the BSS–flow velocity balance is altered, initially showing a more significant sheltering effect at low shell content ($\leq 15\,\%$) as higher shell quantities will disproportionately enhance the turbulence under a flat bed setting. However, when a sufficient flow velocity is achieved to generate ripples, the shell-induced turbulence will quickly be overcome by the developing bedforms and offset the initial trend. The armoring effect grows stronger with increasing shell content in the form of immobile shells.

In terms of sedimentary transport, shell compositions above 15 %–20 % exhibit a drastic change in the ability of ripples to develop and migrate. The threshold is somewhat higher in the constant flow than in the ACC flow experiment (20 % vs. 15 % shell), given the much longer exposure to higher-velocity and equilibrium conditions. A sandy mixture with 2.5 %–50 % shell content increasingly dampens the ripples, thereby reducing the ripple migration by up to 1 order of magnitude. Moreover, these percentages are representative of certain areas within the natural environment. Thus, the presence of shells needs to be taken into account to better understand and predict the sedimentary processes, compared with the more simplistic conditions that could be expected from purely siliciclastic sediment. Our experiments shed some light on the direct influences of shells on ripple dynamics in sandy sediment under unidirectional current-flow conditions. This work would greatly benefit from further studies utilizing other grain sizes combined with shells, as well as an investigation on the other particles of different origin, size, shape and density that are also commonly found throughout the marine environment.

Data availability. The data collected and used for this publication have been deposited in the 4TU.ResearchData repository, hosted by TU Delft, the Netherlands: https://doi.org/10.4121/12852113 (Cheng, 2021).

Supplement. The supplement related to this article is available online at: https://doi.org/10.5194/esurf-9-1335-2021-supplement.

Author contributions. CHC was responsible for conceptualizing the study; developing the methodology; undertaking the investigation, formal analysis and data curation; creating figures; writing, reviewing and editing the paper; and project administration. JCdS was responsible for conceptualizing the study; developing the methodology; undertaking the investigation, formal analysis and software development; creating figures; and writing, reviewing and editing the paper. GSF contributed to developing the methodology; undertaking the formal analysis; developing the software; creating figures; and writing, reviewing and editing the paper. SJMHH contributed to writing, reviewing and editing the paper and was responsible for funding acquisition. BWB was for responsible conceptualizing the study; writing, reviewing and editing the paper; and supervising the study. KS contributed to the conceptualization of the study; writing, reviewing and editing the paper; the supervision of the study; and the acquisition of resources and funding.

Competing interests. The authors declare that they have no conflict of interest.

Disclaimer. Publisher's note: Copernicus Publications remains neutral with regard to jurisdictional claims in published maps and institutional affiliations.

Acknowledgements. The authors would like to thank Tjeerd Bouma for aiding in the planning and conceptualization of the experiment. Lennart van IJzerloo, Bert Sinke and Arne den Toonder are also acknowledged for their assistance with setting up the flume.

Financial support. This research has been supported by the Aard- en Levenswetenschappen, Nederlandse Organisatie voor Wetenschappelijk Onderzoek (grant no. 871.15.011) and also the Aard- en Levenswetenschappen, Nederlandse Organisatie voor Wetenschappelijk Onderzoek, Domein Toegepaste en Technische Wetenschappen (grant no. NWA.1236.18.003).

Review statement. This paper was edited by Daniel Parsons and reviewed by Jaco H. Baas and one anonymous referee.

References

Ahmerkamp, S., Winter, C., Janssen, F., Kuypers, M. M. M., and Holtappels, M.: The impact of bedform migration on benthic oxygen fluxes, J. Geophys. Res.-Biogeo., 120, 2229–2242, https://doi.org/10.1002/2015JG003106, 2015.

Al-Dabbas, M. A. M. and McManus, J.: Shell fragments as indicators of bed sediment transport in the Tay Estuary, P. Roy. Soc. Edinburgh Sect. B, 92, 335–344, https://doi.org/10.1017/S0269727000004759, 1987.

Ashley, G., Boothroyd, J. C., Bridge, J. S., Clifton, H. E., Dalrymple, R., Elliott, T., Flemming, B., Harms, J. C., Harris, P., Hunter, R. E., Kreisa, R. D., Lancaster, N., Middleton, G. V., Paola, C., Rubin, D. M., Smith, J. D., Southard, J. B., Terwindt, J. H. I., and Twitchell, D. C.: Classification of large-scale subaqueous bedforms: a new look at an old problem, J. Sediment Petrol., 60, 160–172, 1990.

Baas, J. H. and De Koning, H.: Washed-out ripples; their equilibrium dimensions, migration rate, and relation to suspended-sediment concentration in very fine sand, J. Sediment Res., 65, 431–435, https://doi.org/10.1306/D42680E5-2B26-11D7-8648000102C1865D, 1995.

Baas, J. H., van Dam, R. L., and Storms, J. E. A.: Duration of deposition from decelerating high-density turbidity currents, Sediment Geol., 136, 71–88, https://doi.org/10.1016/S0037-0738(00)00088-9, 2000.

Bartholdy, J., Ernstsen, V. B., Flemming, B. W., Winter, C., Bartholomä, A., and Kroon, A.: On the formation of current ripples, Sci. Rep., 5, 11390, https://doi.org/10.1038/srep11390, 2015.

Blanchard, G. F., Guarini, J.-M., Gros, P., and Richard, P.: Seasonal effect on the relationship between the photosynthetic capacity of intertidal microphytobenthos and temperature, J. Phycol., 33, 723–728, https://doi.org/10.1111/j.0022-3646.1997.00723.x, 1997.

Borchers, H. W.: pracma: Practical Numerical Math Functions, available at: https://cran.r-project.org/web/packages/pracma/index.html (last access: 8 April 2021), 2019.

Brakenhoff, L., Schrijvershof, R., van der Werf, J., Grasmeijer, B., Ruessink, G., and van der Vegt, M.: From Ripples to Large-Scale Sand Transport: The Effects of Bedform-Related Roughness on Hydrodynamics and Sediment Transport Patterns in Delft3D, J. Mar. Sci. Eng., 8, 1–25, https://doi.org/10.3390/jmse8110892, 2020.

Cheng, C. H.: NIOZ racetrack sand-shell experiment, data belonging to the paper: Sediment shell-content diminishes current-driven sand ripple development and migration, 4TU.ResearchData [data set], https://doi.org/10.4121/12852113, 2021.

Cheng, C. H., Soetaert, K., and Borsje, B. W.: Sediment Characteristics over Asymmetrical Tidal Sand Waves in the Dutch North Sea, J. Mar. Sci. Eng., 8, 1–16, https://doi.org/10.3390/jmse8060409, 2020.

Curran, J. C.: An investigation of bed armoring process and the formation of microclusters, in: 2nd Joint Federal Interagency Conference, Las Vegas, 1–12, 2010.

Damveld, J. H., Reijden, K. J., Cheng, C., Koop, L., Haaksma, L. R., Walsh, C. A. J., Soetaert, K., Borsje, B. W., Govers, L. L., Roos, P. C., Olff, H., and Hulscher, S. J. M. H.: Video transects reveal that tidal sand waves affect the spatial distribution of benthic organisms and sand ripples, Geophys. Res. Lett.,45, 11837–11846, https://doi.org/10.1029/2018GL079858, 2018.

Damveld, J. H., Roos, P. C., Borsje, B. W., and Hulscher, S. J. M. H.: Modelling the two-way coupling of tidal sand waves and benthic organisms: A linear stability approach, Environ. Fluid Mech., 19, 1073–1103, https://doi.org/10.1007/s10652-019-09673-1, 2019.

Dey, S.: Incipient Motion of Bivalve Shells on Sand Beds under Flowing Water, J. Eng. Mech., 129, 232–240, https://doi.org/10.1061/(ASCE)0733-9399(2003)129:2(232), 2003.

Dietrich, W., Kirchner, J., Ikeda, H., and Iseya, F.: Sediment Supply and Development of Coarse Surface Layer in Gravel Bedded Rivers, Nature, 340, 215–217, https://doi.org/10.1038/340215a0, 1989.

Earle, S.: Sea-Floor Sediments, available at: https://geo.libretexts.org/@go/page/7876 (last access: 8 April 2021), 2020.

Friedrichs, M., Graf, G., and Springer, B.: Skimming flow induced over a simulated polychaete tube lawn at low population densities, Mar. Ecol. Prog. Ser., 192, 219–228, https://doi.org/10.3354/meps192219, 2000.

Friedrichs, M., Leipe, T., Peine, F., and Graf, G.: Impact of macrozoobenthic structures on near-bed sediment fluxes, J. Mar. Syst., 75, 336–347, https://doi.org/10.1016/j.jmarsys.2006.12.006, 2009.

Friend, P. L., Lucas, C. H., Holligan, P. M., and Collins, M. B.: Microalgal mediation of ripple mobility, Geobiology, 6, 70–82, https://doi.org/10.1111/j.1472-4669.2007.00108.x, 2008.

Gornitz, V.: Encyclopedia of Paleoclimatology and Ancient Environments, Springer, https://doi.org/10.1007/978-1-4020-4411-3, 2008.

Gutiérrez, J., Jones, C., Strayer, D., and Iribarne, O.: Mollusks as ecosystem engineers: The role of shell production in aquatic habitats, Oikos, 101, 79–90, https://doi.org/10.1034/j.1600-0706.2003.12322.x, 2003.

Herman, P., Middelburg, J., and Heip, C.: Benthic community structure and sediment processes on an intertidal flat: Results from the ECOFLAT project, Cont. Shelf Res., 21, 2055–2071, https://doi.org/10.1016/S0278-4343(01)00042-5, 2001.

Huettel, M. and Rusch, A.: Transport and degradation of phytoplankton in permeable sediment, Limnol. Oceanogr., 45, 534–549, https://doi.org/10.4319/lo.2000.45.3.0534, 2000.

Idier, D., Astruc, D., and Hulscher, S. J. M. H.: Influence of bed roughness on dune and megaripple generation, Geophys. Res. Lett., 31, L13214, https://doi.org/10.1029/2004GL019969, 2004.

Kidwell, S. M.: Palaeobiological and sedimentological implications of fossil concentrations, Nature, 318, 457–460, https://doi.org/10.1038/318457a0, 1985.

Kösters, F. and Winter, C.: Exploring German Bight coastal morphodynamics based on modelled bed shear stress, Geo-Mar. Lett., 34, 21–36, https://doi.org/10.1007/s00367-013-0346-y, 2014.

Langlois, V. and Valance, A.: Initiation and evolution of current ripples on a flat sand bed under turbulent water flow, Eur. Phys. J. E, 22, 201–208, https://doi.org/10.1140/epje/e2007-00023-0, 2007.

Lapôtre, M., Lamb, M., and McElroy, B.: What sets the size of current ripples?, Geology, 45, G38598.1, https://doi.org/10.1130/G38598.1, 2017.

Lichtman, I. D., Baas, J. H., Amoudry, L. O., Thorne, P. D., Malarkey, J., Hope, J. A., Peakall, J., Paterson, D. M., Bass, S. J., Cooke, R. D., Manning, A. J., Davies, A. G., Parsons, D. R., and Ye, L.: Bedform migration in a mixed sand and cohesive clay intertidal environment and implications for bed material transport predictions, Geomorphology, 315, 17–32, https://doi.org/10.1016/j.geomorph.2018.04.016, 2018.

Ligges, U., Short, T., Kienzle, P., Schnackenberg, S., Billinghurst, D., Borchers, H.-W., Carezia, A., Dupuis, P., Eaton, J. W., Farhi, E., Habel, K., Hornik, K., Krey, S., Lash, B., Leisch, F., Mersmann, O., Neis, P., Ruohio, J., Smith, J. O., Stewart, D., and Weingessel, A.: signal: Signal Processing, available at: https://cran.r-project.org/web/packages/signal/index.html (last access: 8 April 2021), 2015.

Malarkey, J., Baas, J. H., Hope, J. A., Aspden, R. J., Parsons, D. R., Peakall, J., Paterson, D. M., Schindler, R. J., Ye, L., Lichtman, I. D., Bass, S. J., Davies, A. G., Manning, A. J., and Thorne, P. D.: The pervasive role of biological cohesion in bedform development, Nat. Commun., 6, 6257, https://doi.org/10.1038/ncomms7257, 2015.

Miedema, S. and Ramsdell, R.: Hydraulic transport of sand/shell mixtures in relation with the critical velocity, Terra Aqua, 122, 18–27, 2011.

Mietta, F., Chassagne, C., Manning, A. J., and Winterwerp, J. C.: Influence of shear rate, organic matter content, pH and salinity on mud flocculation, Ocean Dynam., 59, 751–763, https://doi.org/10.1007/s10236-009-0231-4, 2009.

Nelson, T. R., Voulgaris, G., and Traykovski, P.: Predicting wave-induced ripple equilibrium geometry, J. Geophys. Res.-Oceans, 118, 3202–3220, https://doi.org/10.1002/jgrc.20241, 2013.

Nowell, A. R. M. and Jumars, P. A.: Flow Environments of Aquatic Benthos, Annu. Rev. Ecol. Syst., 15, 303–328, https://doi.org/10.1146/annurev.es.15.110184.001511, 1984.

Paterson, A., Hume, T., and Healy, T.: River Mouth Morphodynamics on a Mixed Sand-Gravel Coast, J. Coast. Res., 34, 288–294, 2001.

Pilditch, C. A., Emerson, C. W., and Grant, J.: Effect of scallop shells and sediment grain size on phytoplankton flux to the bed, Cont. Shelf Res., 17, 1869–1885, https://doi.org/10.1016/S0278-4343(97)00050-2, 1997.

Pope, N., Widdows, J., and Brinsley, M.: Estimation of bed shear stress using the turbulent kinetic energy approach – A comparison of annular flume and field data, Cont. Shelf Res., 26, 959–970, https://doi.org/10.1016/j.csr.2006.02.010, 2006.

Precht, E. and Huettel, M.: Advective pore-water exchange driven by surface gravity waves and its ecological implications, Limnol. Oceanogr., 48, 1674–1684, https://doi.org/10.4319/lo.2003.48.4.1674, 2003.

Ramsdell, R. and Miedema, S.: Hydraulic transport of sand/shell mixtures, in: WODCON XIX, WODA – World Organization of Dredging Associations, Beijing, 1–21, 2010.

R Core Team: R: A language and environment for statistical computing, R Foundation for Statistical Computing, Vienna, Austria, available at: https://www.R-project.org (last access: 8 April 2021), 2020.

Russell-Hunter, W. D. (Ed.): Chapter 1 Overview: Planetary Distribution of and Ecological Constraints upon the Mollusca, in: The Mollusca: Ecology, vol. 6, Academic Press, Orlando, USA, 1–27, 1983.

Seibold, E. and Berger, W. (Eds.): Sources and Composition of Marine Sediments BT – The Sea Floor: An Introduction to Marine Geology, Springer International Publishing, Cham, 45–61, 2017.

Shen, H. W. and Lu, J.: Development and Prediction of Bed Armoring, J. Hydraul. Eng., 109, 611–629, https://doi.org/10.1061/(ASCE)0733-9429(1983)109:4(611), 1983.

Soulsby, R.: Chapter 5 The Bottom Boundary Layer of Shelf Seas, in: Physical Oceanography of Coastal and Shelf Seas, vol. 35, edited by: Johns, B., Elsevier, New York, USA, 189–266, 1983.

Soulsby, R.: Dynamics of Marine Sands: A manual for Practical Applications, Thomas Telford Publishing, London, UK, 1997.

Sugiyama, J. and Kobayashi, K.: wvtool: Image Tools for Automated Wood Identification, available at: https://cran.r-project.org/web/packages/wvtool/index.html (last access: 8 April 2021), 2016.

Tuijnder, A. P., Ribberink, J. A. N. S., and Hulscher, S. J. M. H.: An experimental study into the geometry of supply-limited dunes, Sedimentology, 56, 1713–1727, https://doi.org/10.1111/j.1365-3091.2009.01054.x, 2009.

van Ledden, M., van Kesteren, W. G. M., and Winterwerp, J. C.: A conceptual framework for the erosion behaviour of sand–mud mixtures, Cont. Shelf Res., 24, 1–11, https://doi.org/10.1016/j.csr.2003.09.002, 2004.

Van Oyen, T., de Swart, H. E., and Blondeaux, P.: Bottom topography and roughness variations as triggering mechanisms to the formation of sorted bedforms, Geophys. Res. Lett., 37, 1–5, https://doi.org/10.1029/2010GL043793, 2010.

van Rijn, L. C.: Principles of sediment transport in rivers, estuaries and coastal seas, Aqua Publications Amsterdam, Amsterdam, the Netherlands, 1993.

van Rijn, L. C., Nieuwjaar, M. W. C., van der Kaay, T., Nap, E., and van Kampen, A.: Transport of Fine Sands by Currents and Waves, J. Waterw. Port Coast. Ocean Eng., 119, 123–143, https://doi.org/10.1061/(ASCE)0733-950X(1993)119:2(123), 1993.

Vericat, D., Batalla, R. J., and Garcia, C.: Breakup and reestablishment of the armour layer in a large gravel-bed river below dams: The lower Ebro, Geomorphology, 76, 122–136, https://doi.org/10.1016/j.geomorph.2005.10.005, 2006.

Wilcock, P. and Detemple, B.: Persistence of Armor Layers in Gravel-Bed Streams, Geophys. Res. Lett, 32, L08402, https://doi.org/10.1029/2004GL021772, 2005.

Witbaard, R., Bergman, M. J. N., van Weerlee, E., and Duineveld, G. C. A.: An estimation of the effects of Ensis directus on the transport and burial of silt in the near-shore Dutch coastal zone of the North Sea, J. Sea Res., 127, 95–104, https://doi.org/10.1016/j.seares.2016.12.001, 2016.